Quantitation of Affinity, Avidity, and Binding Kinetics of Protein Analytes with a Dynamically Switchable Biosurface

Jelena Knezevic, Andreas Langer, Paul A. Hampel, Wolfgang Kaiser, Ralf Strasser, and Ulrich Rant*

Walter Schottky Institute & Institute for Advanced Study, Technische Universität München, 85748 Garching, Germany

ⓈSupporting Information

ABSTRACT: A label-free method for the analysis of interactions of proteins with surface-tethered ligands is introduced. Short DNA levers are electrically actuated on microelectrodes by ac potentials, and their switching dynamics are measured in real-time by fluorescence energy transfer. Binding of proteins to ligands attached to the top of the DNA levers is detected by time-resolved measurements of the levers' dynamic motion. We demonstrate the quantitation of binding kinetics (k_{on}, k_{off} rate constants), dissociation constants (K_D in the pM regime), and the influence of competitive binders (EC_{50} values). Moreover, the "switchSENSE" method reveals avidity effects and allows discriminating between analytes with one or more binding sites. In a comparative study, interactions of six hexa-histidine-tagged proteins with tris-nitrilotriacetic acid (NTA_3) ligands are quantitated. Their binding kinetics and affinities are found to vary over up to 2 orders of magnitude, evidencing that the proteins' individual chemical environments significantly influence the His_6–NTA_3 interaction.

Label-free surface biosensors are invaluable tools for the quantitative analysis of molecular interactions between small molecules, nucleic acids, and proteins. While one binding partner (the ligand) is immobilized on the surface, the other (the analyte) flows across the surface in solution. As analyte adsorbs to and accumulates at the surface, it may induce changes in the refractive index,[1,2] mass and elasticity,[3,4] or charge[5–7] of the adlayer. Conventional label-free biosensors measure these macroscopic interface properties averaged over typically square-millimeter areas, akin to the characterization of continuous thin films. Recently, the conformation switching of surface-bound DNA probes has been demonstrated as a versatile sensing modality for the analysis of molecular interactions.[8–12]

Here, we demonstrate a method for detecting molecules on surfaces based on a molecular dynamics measurement. Instead of immobilizing one of the binding partners, the ligands are attached to the upper ends of surface-fixated 16 nm long (48 bp) DNA levers, allowing them to "sway" through the solution. To this end, the negatively charged DNA levers are actuated by ac electric fields, which drive them to oscillate (switch) at frequencies of up to several 100 kHz between a vertical and horizontal orientation on the surface.

Binding of analyte to ligands atop the DNA levers is detected by a time-resolved switching dynamics measurement, which is

introduced in Figure 1A. First, a positive voltage of typically +0.3 V (vs Pt) is applied to the substrate gold electrode, to
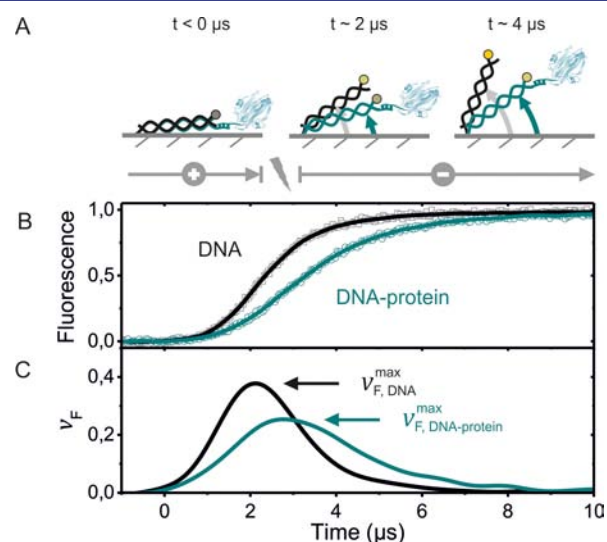

Figure 1. (A) Schematic representation of the DNA lever. Lying on the surface at positive potentials, the DNA is repelled after switching to negative potentials. If a protein is bound to a ligand attached to the DNA's top end, the upward motion is slowed and lags behind the bare lever. The shaded yellow circle symbolizes the Cy3 fluorophore, whose emission is quenched close to the surface. (B) Time-resolved normalized fluorescence of a 48 bp Cy3-labeled DNA before (black) and after (blue) binding protein A (39 kDa). At $t = 0$ μs, the potential is switched from +0.3 to −0.5 V. (C) Time derivative $\nu_F = dF/dt$ of the normalized fluorescence.

which the DNA lever is tethered at one end via a sulfur linker. Attracted by the positive surface charge, the DNA lies on the surface. In this state, the fluorescence emission from Cy3 dyes attached at the surface-distal DNA ends is low, owing to a proximity quenching effect of the metal substrate.[13] When the electrode potential is switched to −0.5 V, the negatively charged DNA is repelled from the surface and pushed upward by virtue of the strong electric field within the developing Gouy–Chapman–Stern screening layer. Simultaneously, the fluorescence emission increases as the Cy3 dyes move away from the quenching surface. The fluorescence emission effectively reports the distance of the DNA's top end to the surface, as described in ref 13.
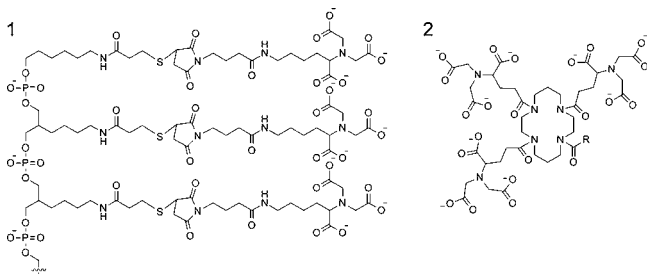
In practice, an epi-fluorescence setup is used to collect the Cy3-fluorescence from approximately 10^6 DNA levers tethered to a $d = 120$ μm circular gold electrode. A counter records single photons and bins them with nanosecond resolution according to their delay times with respect to the negative edge of the applied square wave voltage in a time-correlated single-photon-counting setup. Typically, the DNA switching is driven at 10 kHz, and a fluorescence modulation of 100 kcps is observed (Figure S2). The acquisition of a fluorescence histogram depicting the DNA levers' upward motion takes only seconds.

Figure 1B shows the time-resolved signal of a DNA layer before and after binding a 39 kDa recombinant protein (His-tagged protein A). The upward motion with protein A bound to the DNA lever clearly lags behind the dynamics of the bare layer; that is, the "bulky head" slows the lever motion. This is a consequence of the additional hydrodynamic drag (not mass or moment of inertia) that occurs when the protein binds to the DNA's top end. In fact, the protein diameter can be determined with angstrom resolution by comparing the time-resolved upward dynamics with a statistical treatment of the DNA levers equation of motion, which will be reported elsewhere. With the current setup, proteins with a diameter >2 nm or a molecular weight of approximately >5 kDa can be detected.

To investigate whether quantitative binding information can be obtained from the time-resolved switching measurement, we chose a generic coupling strategy to bind different proteins atop the DNA lever. Tris-nitrilotriacetic acid (tris-NTA, or NTA$_3$) ligands (Chart 1, 1) were conjugated to tris-amino-modified

Chart 1. (1) Linear Tris-NTA Ligand Used in This Work and Ref 14 and (2) Cyclic Tris-NTA Used in Refs 15−18

oligonucleotides following a protocol reported by Turberfield and co-workers[14] (see the Supporting Information for details). Multivalent NTA ligands have been shown to bind histidine-tagged proteins via Ni^{2+} chelation with high affinity, which can be regulated by the addition of competitive binders.[15−19] They are of particular importance as controllable "glue" for biomolecular nanostructures[14,20,21] and surface biosensors.[18,19,22−24]

As an indicator of protein binding, we define a switching velocity parameter based on the measured time-resolved fluorescence, $v_F = dF/dt$, which is related to the mechanical velocity of the DNA lever's top end ($v = dz/dt$). Its maximal value, v_F^{max}, can be easily evaluated (see Figure 1 C) and is used for quantifying the occupancy of surface ligands with analyte. v_F^{max} values without protein, and at sufficiently high protein concentration (saturation conditions), are taken as 0% and 100% ligand occupancy, respectively. Fractional occupancies are obtained from intermediate v_F^{max} values by linear interpolation. In doing so, binding isotherms can be acquired from protein titrations (Figure 2), which reveal dissociation constants, and—
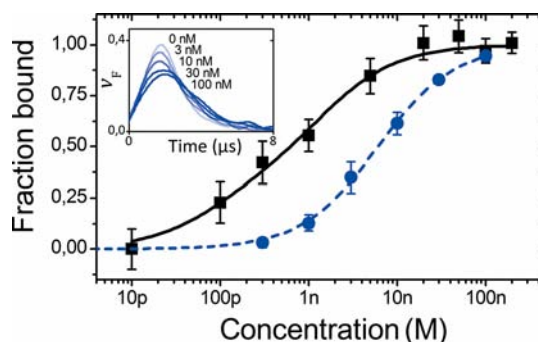

Figure 2. Equilibrium binding isotherms of proteins with one (blue circles, protein G) and two (black squares, protein A) His tags to tris-NTA-modified DNA levers. The dashed fit line is a Langmuir isotherm, the solid fit line is a linear combination of two Langmuir isotherms, see eq 1. Inset: Protein concentration-dependent velocity profiles.

via the shape and steepness of the adsorption curve—the mode of the ligand−analyte interaction (multivalent interactions, presence of inhibitors).

Figure 2 shows how quantitative affinity values and information about the analyte's number of binding sites (avidity effects) are obtained from equilibrium titrations. Blue circles denote the equilibrium binding curve of recombinant protein G (26 kDa) with *one* His$_6$ tag. A Langmuir isotherm (dashed line) perfectly fits the data and yields a dissociation constant $K_D = 6.1 \pm 0.3$ nM. By contrast, the black squares denote binding of protein A with *two* His$_6$ tags, which protrude from the N- and C-terminal, respectively. The progression of this binding curve is not as steep as the other and cannot be fitted with a simple Langmuir isotherm. Instead, a linear combination of two Langmuir terms was used to generate the solid fit line, which yields two K_D values, i.e., $K_{D,1} = 1.5$ nM and $K_{D,2} = 91$ pM.

$$\text{fraction bound} = \sum_{i=1}^{n} A_i \frac{c}{c + K_{D,i}} \tag{1}$$

Equation 1 denotes a linear combination of Langmuir terms, with c being the analyte concentration, A being a (fit) constant, and n being the number of binding sites (here, 1 or 2).

A two-component binding model indicates that interactions between two independent ligand−analyte couples take place on the surface. In the case at hand, some of the double-tagged proteins bind to *one* DNA lever with one of their His$_6$ tags, while some bind simultaneously to *two* DNA levers with both His$_6$ tags (avidity effect). This is a consequence of the extremely low ligand (DNA lever) density, which is a special feature of the electrically switchable DNA layers used here. During the layer preparation, the density of initially adsorbed DNA molecules is being carefully reduced by electrical desorption steps, so that the DNA levers have enough space to freely rotate around their tethers and do not "bump" into each other when lying down on the surface[25,26] (i.e., $d_{DNA−DNA} \geq 2l_{DNA}$, see Supporting Information). In this DNA density regime, some of the DNA levers are still close enough to become interlinked by a protein with two binding tags, while other levers are too far apart to become interlinked. Thus, the binding isotherm of an analyte with two binding sites reflects single as well as double interactions, namely 1:1 (high K_D) and 1:2 (low K_D) protein:DNA lever binding stoichiometries. [Note that the special shape of the isotherm is not caused by
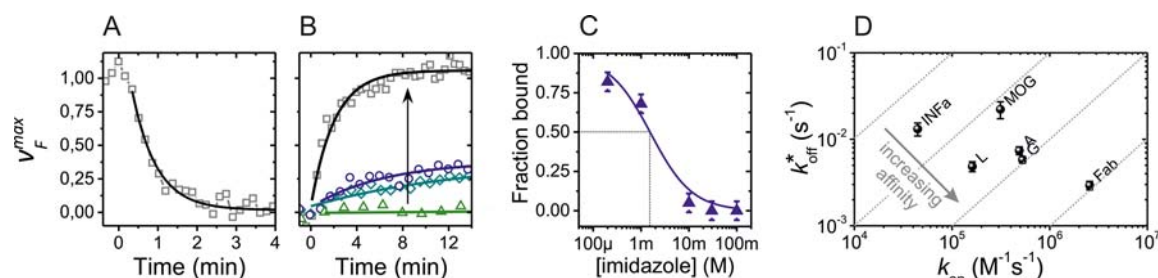
Figure 3. Binding kinetics measurements. (A) Binding of protein A (50 nM) to trisNTA modified DNA levers monitored in real-time by the change in the switching velocity v_F. The solid line is an exponential fit. (B) Unbinding kinetics as a function of imidazole concentration, 0, 0.2, 1, and 100 mM (see arrow). (C) Fraction of bound protein after 10 min incubation in different imidazole concentrations. $EC_{50} = 1.8 \pm 0.4$ mM. (D) Reaction rate map. k_{on} and k_{off}^* were determined in 50 nM protein solutions and 10 mM imidazole solutions, respectively. Dotted lines are quasi iso-affinity lines ($k_{on}/k_{off}^* =$ const.).

different binding affinities of the two distinct N- and C-terminal His_6 tags. In an equilibrium titration experiment, where the analyte concentration is increased stepwise, the weaker His_6 tag does not become apparent individually in the binding isotherm as a sole binder. Surface ligands get occupied with proteins binding via the strong-affinity tag already at concentrations which are too low for the weaker tag to bind. Thus, the binding curve must resemble a pseudo one-component Langmuir isotherm, reflecting the affinity of the stronger tag.] Moreover, for sensing purposes, low-density layers are generally advantageous because of their favorable probe accessibility.[27]

Reaction kinetics are investigated by monitoring v_F^{max} in real-time. Figure 3A shows the binding of protein A, pumped in a fluidic channel across a NTA_3-DNA modified electrode. The v_F^{max} time course can be fitted well with a single exponential function, which indicates reaction-limited association kinetics[28] with an association rate $k_{on} = (4.7 \pm 0.3) \times 10^5$ M^{-1} s^{-1}. The reaction limited regime was confirmed by varying the volumetric flow rate (mass transport) by an order of magnitude, which left the association time constant τ_{on} unchanged (Figure S3). Further, as expected for first-order binding kinetics ($\tau_{on}^{-1} = ck_{on} + k_{off}$), a linear dependence of τ_{on}^{-1} on the protein concentration c was confirmed experimentally (Figure S4). The unbinding of His_6-tagged proteins from NTA_3 was found to be very slow ($k_{off} = \tau_{off}^{-1} \approx 10^{-4}$ s^{-1}); after 3.5 h, only 10% of the initially bound protein A had dissociated from the DNA layer. Thus, this scheme is well suited to be used in a protein−protein interaction assay, where one of the proteins is immobilized via the NTA_3-His_6 coupling (cf. Figure S8).

The influence of a competitive binder on the dissociation rate of His_6-tagged proteins from NTA_3-DNA levers was investigated by exposing the layers to a flow of imidazole (0−100 mM). As imidazole competes with histidine for chelating NTA bound Ni^{2+} ions, increasing imidazole concentrations resulted in faster unbinding (Figure 3B); 30 mM imidazole sufficed to induce complete dissociation within a few minutes. Concentration-dependent dissociation curves were evaluated for an exposure time of 10 min, yielding an imidazole half-maximum effective concentration $EC_{50} = 1.8 \pm 0.4$ mM (Figure 3C).

The kinetic rate constants and dissociation constant mentioned above are in agreement with literature reports[14−18] about other His_6-tagged proteins and structurally different tris-NTA modifiers, where the NTA moieties are attached to a cyclic scaffold rather than in a linear fashion like here (Chart 1). However, as literature values differ substantially, we investigated

the variability in binding kinetics for different proteins. Association curves were recorded for recombinant, His_6-tagged versions of interferon alpha (INFα), myelin oligodendrocyte glycoprotein (MOG), protein A, protein G, protein L, and a monoclonal IgG fragment (Fab). Dissociation was performed in 10 mM imidazole flow, so that unbinding curves could be acquired within minutes. The obtained k_{on} and k_{off}^* values are summarized in the reaction rate map in Figure 3D (raw data and fits are shown in Figure S5).

We found that the individual nature of a protein dramatically affects the ability of its His_6 tag to bind to the NTA_3 ligand: the k_{on} values of the six investigated proteins span 2 orders of magnitudes, their k_{off}^* values range over 1 order of magnitude. These results are supported by surface plasmon resonance measurements (Figure S7, Table S3). In particular, the wide range of k_{on} values points to the fact that the accessibilities of individual His tags are very dissimilar. As a general trend, the rate map suggests that fast association (high k_{on}) is correlated with slow dissociation (low k_{off}^*), that is, good accessibility of the His_6 tag entails strong, long-lasting binding. However, contrary to this trend, a comparison of protein L with MOG shows that, although MOG binds faster, L binds stronger. In the latter case, the local chemical environment of protein L surrounding its His_6 tag obviously stabilizes the His_6−NTA_3 interaction.

In conclusion, molecular interactions could be analyzed for the first time by measuring the dynamic motion of electrically actuated surface-tethered molecules. The probe-target switching velocity proved to be a robust sensing parameter, reliably reporting the binding status of *active* (switching) surface probes. Because the scheme does not rely on the measurement of absolute fluorescence intensities, it is not very susceptible to detrimental effects like fluorescence bleaching. Molecular reaction rates, equilibrium binding affinities, and EC_{50} values could be determined quantitatively. Since the scheme involves extremely low probe densities (approximately 10^{10} molecules/cm^2), it is possible to gauge avidity effects. Only one-fourth to one-half of bivalent targets bound to the surface can interlink two probes, which leads to characteristic adsorption isotherms reflecting the simultaneous presence of $T \cdot P$ and $T \cdot P_2$ complexes. The microelectrodes used in this study can be easily arrayed on a single chip for parallel readout of multiple interactions.

ASSOCIATED CONTENT

S **Supporting Information**

Additional association/dissociation curves, concentration-dependent association times, fit models, and materials and methods. This material is available free of charge via the Internet at http://pubs.acs.org.

AUTHOR INFORMATION

Corresponding Author

rant@tum.de

Notes

The authors declare the following competing financial interest(s): W.K., R.S., and U.R. are co-founders of Dynamic Biosensors GmbH, a start-up company recently established in Munich, which aims to commercialize biosensors based on electrically switchable DNA probes in the future.

ACKNOWLEDGMENTS

REFERENCES

(1) Nirschl, M.; Reuter, F.; Vörös, J. *Biosensors* **2011**, *1*, 70.

(2) Abbas, A.; Linman, M. J.; Cheng, Q. *Biosens. Bioelectron.* **2011**, *26*, 1815.

(3) Cheng, C. I.; Chang, Y. P.; Chu, Y. H. *Chem. Soc. Rev.* **2012**, *41*, 1947.

(4) Länge, K.; Rapp, B.; Rapp, M. *Anal. Bioanal. Chem.* **2008**, *391*, 1509.

(5) Grieshaber, D.; MacKenzie, R.; Voeroes, J.; Reimhult, E. *Sensors* **2008**, *8*, 1400.

(6) Lee, C. S.; Kim, S. K.; Kim, M. *Sensors* **2009**, *9*, 7111.

(7) Katz, E.; Willner, I. *Electroanalysis* **2003**, *15*, 913.

(8) Lubin, A. A.; Plaxco, K. W. *Acc. Chem. Res.* **2010**, *43*, 496.

(9) Ricci, F.; Adornetto, G.; Moscone, D.; Plaxco, K. W.; Palleschi, G. *Chem. Commun.* **2010**, *46*, 1742.

(10) Farjami, E.; Clima, L.; Gothelf, K.; Ferapontova, E. E. *Anal. Chem.* **2011**, *83*, 1594.

(11) Rant, U.; Arinaga, K.; Scherer, S.; Pringsheim, E.; Fujita, S.; Yokoyama, N.; Tornow, M.; Abstreiter, G. *Proc. Natl. Acad. Sci. U.S.A.* **2007**, *104*, 17364.

(12) Rant, U.; Pringsheim, E.; Kaiser, W.; Arinaga, K.; Knezevic, J.; Tornow, M.; Fujita, S.; Yokoyama, N.; Abstreiter, G. *Nano Lett.* **2009**, *9*, 1290.

(13) Kaiser, W.; Rant, U. *J. Am. Chem. Soc.* **2010**, *132*, 7935.

(14) Goodman, R. P.; Erben, C. M.; Malo, J.; Ho, W. M.; McKee, M. L.; Kapanidis, A. N.; Turberfield, A. J. *Chembiochem* **2009**, *10*, 1551.

(15) Lata, S.; Reichel, A.; Brock, R.; Tampé, R.; Piehler, J. *J. Am. Chem. Soc.* **2005**, *127*, 10205.

(16) Lata, S.; Gavutis, M.; Tampé, R.; Piehler, J. *J. Am. Chem. Soc.* **2006**, *128*, 2365.

(17) Huang, Z.; Park, J. I.; Watson, D. S.; Hwang, P.; Szoka, F. C., Jr. *Bioconjugate Chem.* **2006**, *17*, 1592.

(18) Huang, Z.; Hwang, P.; Watson, D. S.; Cao, L.; Szoka, F. C., Jr. *Bioconjugate Chem.* **2009**, *20*, 1667.

(19) Valiokas, R.; Klenkar, G.; Tinazli, A.; Reichel, A.; Tampe, R.; Piehler, J.; Liedberg, B. *Langmuir* **2008**, *24*, 4959.

(20) Selmi, D. N.; Adamson, R. J.; Attrill, H.; Goddard, A. D.; Gilbert, R. J. C.; Watts, A.; Turberfield, A. J. *Nano Lett.* **2011**, *11*, 657.

(21) Shen, W.; Zhong, H.; Neff, D.; Norton, M. L. *J. Am. Chem. Soc.* **2009**, *131*, 6660.

(22) Nieba, L.; Nieba-Axmann, S. E.; Persson, A.; Hämäläinen, M.; Edebratt, F.; Hansson, A.; Lidholm, J.; Magnusson, K.; Karlsson, Å. F.; Plückthun, A. *Anal. Biochem.* **1997**, *252*, 217.

(23) Andre, T.; Reichel, A.; Wiesmueller, K.-H.; Tampe, R.; Piehler, J.; Brock, R. *Chembiochem* **2009**, *10*, 1878.

(24) Alonso, J. M.; Reichel, A.; Piehler, J.; del Campo, A. *Langmuir* **2007**, *24*, 448.

(25) Arinaga, K.; Rant, U.; Knezevic, J.; Pringsheim, E.; Tornow, M.; Fujita, S.; Abstreiter, G.; Yokoyama, N. *Biosens. Bioelectron.* **2007**, *23*, 326.

(26) Rant, U.; Arinaga, K.; Fujita, S.; Yokoyama, N.; Abstreiter, G.; Tornow, M. *Nano Lett.* **2004**, *4*, 2441.

(27) Biagiotti, V.; Porchetta, A.; Desiderati, S.; Plaxco, K. W.; Palleschi, G.; Ricci, F. *Anal. Bioanal. Chem.* **2012**, *402*, 413.

(28) Squires, T. M.; Messinger, R. J.; Manalis, S. R. *Nat. Biotechnol.* **2008**, *26*, 417.

15228

dx.doi.org/10.1021/ja3061276 | *J. Am. Chem. Soc.* 2012, 134, 15225–15228